IEEE Access
Multidisciplinary | Rapid Review | Open Access Journal

Received November 30, 2019, accepted December 17, 2019, date of publication December 27, 2019,
date of current version January 6, 2020.

Digital Object Identifier 10.1109/ACCESS.2019.2962742

Predictive Current Trajectory Control for PMSM at Voltage Limit

GENJI PEI[1], LIYI LI[1], (Senior Member, IEEE), XIAONAN GAO[2], JIAXI LIU[1], AND RALPH KENNEL[2], (Senior Member, IEEE)

[1]Harbin Institute of Technology, Harbin 150001, China
[2]Institute for Electrical Drive Systems and Power Electronics, Technical University of Munich, 80333 Munich, Germany

Corresponding author: Liyi Li (liliyi.hit@gmail.com)

This work was supported in part by the National Science Foundation of China under Grant 51577038, in part by the Key R&D Plan of Guangdong Province under Grant 2019B090917003, and in part by the Science and Technology Planning Project of Guangdong Province under Grant 2017B09091009.

ABSTRACT This paper presents a fast predictive current trajectory strategy for permanent magnet synchronous motors (PMSMs) at voltage limit. The current hexagon obtained from the voltage hexagon of the inverter represents the region that the currents can reach in the next switching periond. The nearest avaliable current point to the reference is solved by geometrical method on the current plane. The output of the proposed algorithm is divided into four cases according to the position of the current points. The algorithm combines FCS-MPC and DPCC, has the merits of both method and also the fast dynamic at voltage limits. In order to increase the robustness against the parameter variations, moving horizon estimator is utilized. The rotor flux is eliminated in the algorithm and the voltage errors caused by resistance and inductance mismatches are compensated by the estimator. Several experiments are performed with DPCC, FCS-MPC and the predictive current trajectory control method. These comparisons validate the effectiveness of the proposed method.

INDEX TERMS Disturbance observer, geometrical solution, PMSM, predictive control, voltage limit.

I. INTRODUCTION

In many industrial applications, especially high-performance ac motor drives, permanent magnet synchronous motors (PMSMs) are widely used for the merits of high power denisty and good control performance. The current loop is the innest part of the control system and produces voltage reference. However, if the high current dynamic is required and a large current command occurs, the calculated voltages from the current regulators may easily go beyond the limits of the DC-link voltage and the current regulators may be seriously saturated [1]. To avoid the performance deteriation and improve the dynamic, a well-designed current regulator is necessary.

Predictive control attracts much interest due to its fast dynamic and simple structure [2]. As one of the predictive control method, deadbeat control aims to control the states to track the reference values at the end of the switching period, by solving the volt-second vector based on the mathematical model. There are two kinds of deadbeat control for PMSM drives, deadbeat direct torque and flux control (DB-DTFC) [3], [4], and deadbeat predictive current control (DPCC) [5]. Deadbeat control is a high bandwidth feedback control method which calculates the reference voltages directly by the model. However, like other vector control methods, the performance is limited when the available voltage is insufficient [6], i.e. the current command cannot be achieved in one control period due to the voltage limit. When the current command is large, the output voltage is saturated and the couple of the *dq*-axis currents becomes large.

Finite control set model predictive control (FCS-MPC) predicts the currents with the basic voltage vectors. Then the vector which minimizes the cost function is selected and directly applied to the inverter. Without a modulator, the switching frequency is variable and the current harmonic is large. Some new structures and improvements have been proposed to address this issue. Ref [7] extends more candidate voltage vectors to make the prediction more accurate, and reduce the torque ripple. A new method, in [8] and [9], is proposed to minimize the cost function and reduce the harmonic with a deadbeat solution. However, the control ability at the physical limits is not concerned in these work. In this work, the MPC and DPCC are well combined in a new predictive strategy for good performance, and the dynamic at limits is considered.

The associate editor coordinating the review of this manuscript and approving it for publication was Jinquan Xu.

To improve the current control performance at current and voltage limits, many methods have been proposed. Anti-windup is an intuitive method to avoid voltage saturation [10], [11]. Since the voltage references cannot be linearly synthesized in this condition, the current tracking performance is significantly degraded. Feedback method [1], [12] has a simple concept to avoid the voltage saturation. This is achieved by alleviating the voltage deficiency with a current feedback scheme. In [1], d-axis current is intensified in the transient state of the PI regulator to secure the voltage margin. The settling time is reasonable reduced.

Time-optimal control at voltage and current limits are researched in DB-DTFC [6], [13], [14]. In [6], a minimum-time ramp trajectory method is proposed as a suboptimal control algorithm for DB-DTFC IPMSM drives to improve transient torque response at voltage limits. In [14], a time optimal torque trajectory method is proposed using dynamic programming and pontryagin's maximom principle as its optimization methods. The fast transient dynamics and deadbeat response at every PWM instant can be achieved along the time optimal trajectory.

Moreover, the idea of using derivative and extremum is used in [15]. The method obtains the voltage vector for a fast torque response by calculating the partial derivative of torque to d-axis voltage. The obtained formula maximizes the torque change in each sampling time. References [16], [17] process the voltage feedback information and obtain geometrical optimization algorithms to select the constraint-optimal dq-current setpoint adjustments. The algorithm has a fast dynamic in torque response. Reference [18] presents four differnet real-time strategies on the current, flux linkage and voltage plane to visulize the physics of the machine dynamics. These four strategies control the system with different targets for fast torque response or time minimization to reach current reference. Reference [19] operates the time-optimal control for current trajectory and presents the numerical solution. Referencce [20] utilizes Pontryagin's Maximum Principle to obtain the time-minimum current trajectory.

It is a drawback of the model-based methods that the algorithm relies on the accuracy of the model parameters. A common solution in predictive control is to use a disturbance observer (DOB) [21]. Different observation methods are used to improve the robustness, e.g. extend kalman filter (EKF) [22], sliding-mode observer (SMO) [23], extended states observer (ESO) [24]. Moving horizon estimator (MHE) is a new method compared with the methods mentioned above. It can provide a robust and stable estimation in case of convergent process and measurement disturbances, due to its full information version [25], [26]. Recently, MHE is used as a high bandwidth estimator for sensorless control of PMSM in [27] and [28]. Reference [29] uses the MHE theory to estimate the rotating nonlinearties of the PMSM. In this paper, we present a MHE algorithm to estimate the back-EMF and disturbance due to its high bandwidth performance.

In this paper, we propose a current trajectory optimization strategy based on predictive control with MHE. The algorithm is described on the dq-axis current plane and solved with geometrical method, which is a simple and intuitive way to express the machine variables and dynamics. The current and voltage limits are considered in the proposed method. Different from the other methods, the basic current hexagon, within which the current points can be reached in next control period, is first obtained with the basic voltage vectors of the inverter. Then, the relative position of the reference current point and the current hexagon is defined in four cases, and the solutions are operated separately. The proposed strategy calculates the regulating capability at every operating point in the discrete domain without the deriatives of the voltage or the torque. It switches freely between two predictive control method, i.e. DPCC and FCS-MPC in transient state and also has good control performance in steady states. Moreover, to increase the robustness of the system against the parameter variations, a moving horizon estimator (MHE) is utilized to estimate the disturbance. Therefore, the back-emf term including the flux-linkage is eliminated in the algorithm and the influence of the parameter mismatches is compensated.

This paper is orgnized as follows. Section II introduces the mathematical equations of PMSM and the basic knowledge of DPCC and FCS-MPC. Section III presents the algorithm of MHE and updates the control model. In section IV, the proposed current control strategy is elaborated. Section V provides the experiments results to validate effectiveness of the proposed method. Section VI concludes the work.

II. MOTOR MODEL AND PREDICTIVE CONTROL METHODS

A. MACHINE MATHEMATICAL MODEL

The voltage equations of PMSM in the rotating reference frame (dq-axis) are presented as (1).

$$\begin{cases} u_d = R_s i_d + L_d d\dfrac{i_d}{dt} - \omega_e L_q i_q \\ u_q = R_s i_q + L_q d\dfrac{i_q}{dt} + \omega_e L_d i_d + \omega_e \psi_f \end{cases} \tag{1}$$

where $\omega_e = p\omega_m$ is the electrical angular speed. ω_m and p are the rotor speed and polepairs. R_s, L_d, L_q, ψ_f are the phase resistance, inductance of d-axis, q-axis and the rotor flux linkage, respectively. The electromagnet torque can be controlled through the dq-axis currents by:

$$T_e = \frac{3}{2} p\psi_f (i_q + (L_d - L_q) i_d i_q) \tag{2}$$

The predictive controller design and the digital process require a discrete machine model. The most commonly used discretization method in motor control is forward Euler method, i.e. at the kth sampling instance, $d\frac{i_d}{dt} = \frac{i_d[k+1]-i_d[k]}{T_s}$, where T_s is the sampling time and the time for executing the control algorithm. The discrete-time model in dq-axis is expressed in (3):

$$\begin{bmatrix} i_d[k+1] \\ i_q[k+1] \end{bmatrix} = A \begin{bmatrix} i_d[k] \\ i_q[k] \end{bmatrix} + B \begin{bmatrix} u_d[k] \\ u_q[k] \end{bmatrix} + D[k] \tag{3}$$

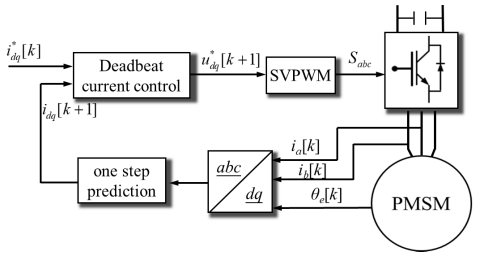

FIGURE 1. The block diagram of DPCC.

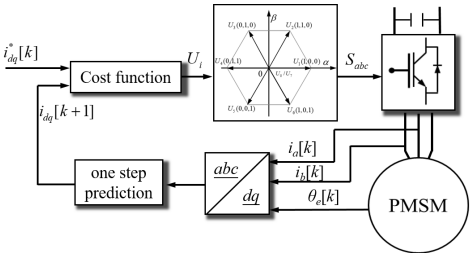

FIGURE 2. The block diagram of FCS-MPC.

where

$$A = \begin{bmatrix} 1 - \dfrac{R_s}{L_s}T_s & \omega_e[k]T_s \\ -\omega_e[k]T_s & 1 - \dfrac{R_s}{L_s}T_s \end{bmatrix},$$

$$B = \begin{bmatrix} \dfrac{T_s}{L_s} & 0 \\ 0 & \dfrac{T_s}{L_s} \end{bmatrix}, \quad D[k] = \begin{bmatrix} 0 \\ \dfrac{\omega_e[k]\psi_f T_s}{L_s} \end{bmatrix}$$

B. DEADBEAT PREDICTIVE CURRENT CONTROL

Deadbeat predictive current control aims to make the motor currents track the references in the next sampling instant by calculating a proper voltage command. According to the DB theory, the reference voltages can be obtained by replacing the predictive currents with the reference currents as (4):

$$\begin{bmatrix} u^*_d[k] \\ u^*_q[k] \end{bmatrix} = B^{-1}\left(\begin{bmatrix} i^*_d \\ i^*_q \end{bmatrix} - A \begin{bmatrix} i_d[k] \\ i_q[k] \end{bmatrix} - D[k] \right) \tag{4}$$

These voltages will be implemented by the modulator at next sampling instant in the digital system. Therefore, one-step prediction is performed in predictive control methods to reduce the digital time delay. Otherwise, overshoots and oscillations will appear. The brief block diagram of DPCC in dq-axis is shown in Fig.1. In the DPCC of dq-axis, the currents at $k+1$th instant is first obtained with (3) for the one-step prediction. Then the reference voltages are modified as:

$$\begin{bmatrix} u^*_d[k+1] \\ u^*_q[k+1] \end{bmatrix} = B^{-1}\left(\begin{bmatrix} i^*_d \\ i^*_q \end{bmatrix} - A \begin{bmatrix} i_d[k+1] \\ i_q[k+1] \end{bmatrix} - D[k+1] \right) \tag{5}$$

C. FINITE CONTROL SET MODEL PREDICTIVE CONTROL

Finite Control Set Model Predictive Control is one of the direct control strategies for electric drives. The method predicts the machine variables with the feasible voltage vectors of the inverter. The optimal voltage vector, which is to be applied in the next sampling period, is selected with a cost function. The design of the cost function decides the control performance of the method. The brief block diagram of FCS-MPC is shown in Fig. 2. In a 2-level voltage source inverter, 8 basic voltage vectors ($U_j, j = 0, 1..7$) are used in the basic FCS-MPC. The equivalent dq-axis voltages are calculated with each switching state S_{abc}, then the predicted dq-axis currents i_{dj}, i_{qj} can be obtaied with the different voltages and (3).

The cost function for current control is usually designed as:

$$g_j = \left| i^*_d(k) - i_{dj}(k) \right| + \left| i^*_q(k) - i_{qj}(k) \right| \tag{6}$$

The jth voltage vector U_j which minimizes the cost function will be selected to operated by the inverter. Note that one-step prediction also needs to be implemented to reduce the influence of digital time delay.

III. DISTURBANCE ESTIMATION WITH MOVING HORIZON ESTIMATOR

It is one of the drawbacks of model-based control method (DPCC and MPC) that the algorithms are sensitive to the parameters and the disturbance. In this work, we use the MHE to estimate the disturbance due to its fast dynamic. The estimated disturbance are the voltage terms including the back-EMF and the voltage errors caused by the parameter mismatches. The moving horizon estimator is operated with a fixed horizon N and a cost function for optimization. It estimates the states with the information of the past N periods.

A. THE MODEL OF MHE

The voltage equations in dq-axis with disturbance (f_d, f_q) is written as follows [21].

$$\begin{cases} u_d - f_d = R_{s0} i_d + L_{s0} \dfrac{di_d}{dt} - L_{s0}\omega_e i_q \\ u_q - f_q = R_{s0} i_q + L_{s0} \dfrac{di_q}{dt} + L_{s0}\omega_e i_d \end{cases} \tag{7}$$

where $R_{s0} = R_s - \Delta R$; $L_{s0} = L_s - \Delta L_s$ and subscript '$_0$' denotes the nominal value. Taken the unmodeled uncertainties $\varepsilon_d, \varepsilon_q$ into consideration, the disturbance can be expressed as:

$$\begin{cases} f_d = \Delta R i_d + \Delta L_s \dfrac{di_d}{dt} - \Delta L_s i_q \omega_e + \varepsilon_d \\ f_q = \Delta R i_q + \Delta L_s \dfrac{di_q}{dt} + \Delta L_s i_d \omega_e + \omega_e \psi_f + \varepsilon_q \end{cases} \tag{8}$$

$\psi_f = \psi_{f0} + \Delta\psi_f$. Note that the back-EMF term is included in f_q, therefore, the flux is elimated in the equations. Replacing $D[k]$ with the estimated term, the model with parameter mismatches can be expressed as:

$$x[k+1] = A_0 x[k] + B_0(u[k] - f[k]) \tag{9}$$

where $x[k] = [i_d[k], i_q[k]]^T$, $u[k] = [u_d[k], u_q[k]]^T$, $f[k] = [f_d[k], f_q[k]]^T$ is the disturbance term. A_0, B_0 are the new matrixes, which replace the parameters R_s, L_s in A, B

with nominal values R_{s0}, L_{s0}. The extended observer model is:

$$\begin{cases} \hat{x}[k+1] = A_0\hat{x}[k] + B_0(u[k] - \hat{f}[k]) \\ \hat{f}[k] = \hat{f}[k-1] + \Delta\hat{f}[k-1] \end{cases} \tag{10}$$

Then the MHE model can be obtained with the extended models of the past N sampling periods.

$$\hat{X} = \Phi\hat{x}_0 + \Gamma(U - \hat{F} - \Delta\hat{F}) \tag{11}$$

where $\hat{X} = [\hat{x}_{[k-N+1]}, \cdots, \hat{x}_{[k+1]}]^T$ is the states vector, $\hat{x}_0 = \hat{x}_{k-N}$. $U = [u_{[k-N]}, \cdots, u_{[k]}]^T$ is the control vector, $\hat{F} = [\hat{f}_{[k-N-1]}, \cdots, \hat{f}_{[k-1]}]^T$ is the disturbance vector, and $\Delta\hat{F}$ is the increment of the disturbance, which is also the optimation result of the cost function. Φ and Γ are the extended matrixes after the iteration.

$$\Phi = \begin{bmatrix} A_0 \\ \vdots \\ A_0^{N+1} \end{bmatrix}, \quad \Gamma = \begin{bmatrix} B_0 & 0 & \cdots & 0 \\ A_0B_0 & B_0 & \cdots & 0 \\ \vdots & \vdots & \ddots & 0 \\ A_0^NB_0 & A_0^{N-1}B_0 & \cdots & B_0 \end{bmatrix}$$

B. THE OPTIMIZATION SOLUTION

The cost function J is designed as a quadratic form to value the performance.

$$J = (X - \hat{X})^T(X - \hat{X}) + \Delta\hat{F}^T\Lambda\Delta\hat{F} \tag{12}$$

where $X = [x_{[k-N+1]}, \cdots, x_{[k+1]}]^T$ is the measured actual states. The first term values the errors between the measured currents and the estimated currents. The second term is a restriction of increment of the estimated disturbance. $\Lambda = diag(\lambda_1 I_2, \cdots, \lambda_{N+1} I_2)$ is the weighting matrix, which influences the convergence performance of the estimator. I_2 is 2×2 identity matrix. To obtain the optimal control term $\Delta\hat{F}$, a linear quadratic problem is stated as:

$$\begin{aligned} &\min J(\hat{X}, \Delta\hat{F}) \\ &\text{s.t. } \hat{X} = \Phi\hat{x}_0 + \Gamma(U - \hat{F} - \Delta\hat{F}) \end{aligned}$$

The cost function J can get the minimum value when its gradient to $\Delta\hat{F}$ equals zero:

$$\frac{\partial J}{\partial \Delta\hat{F}} = 0 \tag{13}$$

By substituting (11), (12) into (13), the optimal result of $\Delta\hat{F}$ can be expressed as:

$$\Delta\hat{F} = -\left(2\Gamma^T\Gamma + \Lambda\right)^{-1} \cdot \left(2H^T\Gamma\right)^T \tag{14}$$

where $H = X - \Phi\hat{x}_0 - \Gamma(U - \hat{F})$. The output of MHE $\hat{f}$ is the $N+1$th term of $\hat{F} + \Delta\hat{F}$. In this work, due to the computation burden, the number of N is set as 1.

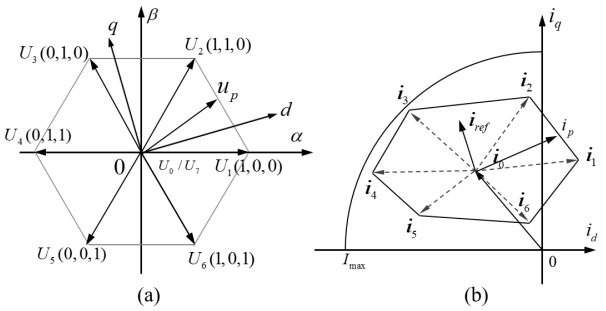

FIGURE 3. Symbol for the hexagons and the operating points. (a) basic voltage hexagon in the voltage plane. (b) basic current hexagon in the current plane.

IV. PREDICTIVE CURRENT CONTROL WITH GEOMETRICAL SOLUTION

DPCC and FCS-MPC have the merit of fast dynamic because of the model-based characteristic. However, the performance will be degraded when the calculated voltages beyond the limits. In this section, a hybrid control strategy is proposed and the nearest current point to the reference is solved every period.

A. CURRENT COMMAND SETPOINT

A current regulator, which is usually used as the inner loop of the speed and motion control, aims to find the appropriate voltages to drive the motor currents from the current values to the command points. Given a $dq-$axis current request, the command setpoint for the regulator is a certain point with the commanded $dq-$axis current values, (i_{dcom}, i_{qcom}). Given a torque request, the $dq-$axis current commands are infinite. Considering the copper loss and the temperature rise, the desirable current references i_{dcom}, i_{qcom} can be obtained with MTPA trajectory as (15) [30]. Where i_s is the stator phase current.

$$\begin{cases} i_{dcom} = \dfrac{\psi_f - \sqrt{\psi_f^2 + 8\left(L_q - L_d\right)^2 i_s^2}}{4\left(L_q - L_d\right)} \\ i_{qcom} = \pm\sqrt{i_s^2 - i_{dcom}^2} \end{cases} \tag{15}$$

B. GEOMETRICAL DESCRIPTION WITH CONSTRAINT PROBLEM

To improve the performance at the operating points near the current and voltage limits, we propose a hybrid predictive control strategy and obtain the solution with geometrical description on the dq-axis current plane.

Fig. 3 shows the basic voltage and current hexagon in the $\alpha\beta$-axis voltage and dq-axis current plane, respectively. The current point at the current instant is $\boldsymbol{i}_0(i_{d0}, i_{q0})$. With one-step prediction, $i_{d0} = i_d[k+1]$, $i_{q0} = i_q[k+1]$. This paper uses one bold letter to express the current point on the plane or the vector from origin to the point, two bold letters to express the vector from the first point to the second one and $|\cdot|$ to express the length of the vector. The radius I_{max} of the current circle is the maximum allowable current of

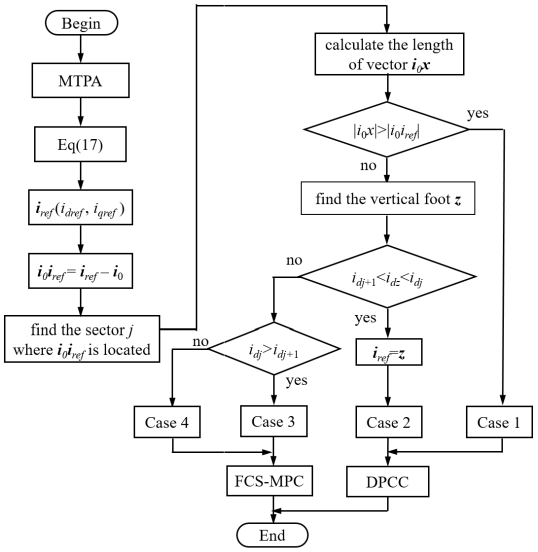

FIGURE 4. Flowchart of the proposed predictive control method.

the system. The six basic current vectors $\boldsymbol{i_0 i_j}$ $(j = 1, 2, \ldots 6)$ in (b) correspond to the basic voltage vectors $\boldsymbol{U}_j$ in (a). The predicted current vertexes $\boldsymbol{i}_j(i_{dj}, i_{qj})$ can be obtained with estimated disturbance and (9).

The points in the current hexagon and the points in the voltage hexagon correspond to each other. Taken point $\boldsymbol{u}_p$ on the side as an example, the point in dq-axis is $\boldsymbol{u}_p = (\lambda \boldsymbol{U}_1 + (1 - \lambda)\boldsymbol{U}_2)e^{-j\theta}$. Considering the steady-state, the voltage equation can be expressed as $\boldsymbol{u} = (R_s + j\omega_e L_s)\boldsymbol{i} + \boldsymbol{\Phi}$. Then the correspond point $\boldsymbol{i}_p$ on the current plane is:

$$\begin{aligned} \boldsymbol{i}_p &= \frac{\boldsymbol{u}_p - \boldsymbol{\Phi}}{R_s + j\omega_e L_s} = \frac{(\lambda \boldsymbol{U}_1 + (1 - \lambda \boldsymbol{U}_2))\, e^{-j\theta} - \boldsymbol{\Phi}}{R_s + j\omega_e L_s} \\ &= \lambda \boldsymbol{i}_1 + (1 - \lambda)\boldsymbol{i}_2 \end{aligned} \tag{16}$$

In this way, the basic current hexagon shows the available current region which can be reached in the next period with the inverter voltage. However, when the current change is large, namely the reference current point is outside the hexagon, the saturation will occur and the performance will be degraded. The proposed predictive control method aims to find the optimal current points within or on the hexagon. The flow chart of the algorithm is shown in Fig. 4 and the steps are listed and introduced as following.

1) DETERMINE THE CURRENT REFERENCE

The reliable current points must be within the current limit. For a current reference, the point can be set directly on the plane. For a torque command, the current reference is first selected with MTPA (15) and then the target changes to the current point tracking problem. If the original current command $\boldsymbol{i}_{com}$ is outside the circle, it cannot be reached without violating the constraint. The command setpoint is selected on the current circle along the direction of the vector $\boldsymbol{i}_{com} = (i_{dcom}, i_{qcom})$. Then the command setpoint

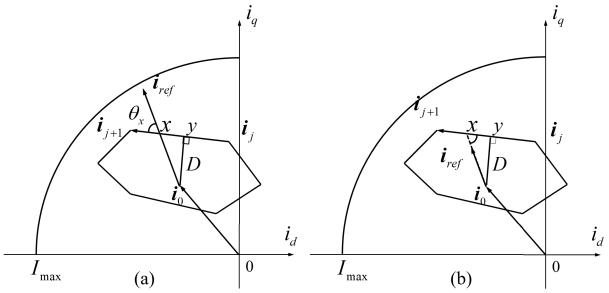

FIGURE 5. Determine the position of i_{ref}. (a) outside the hexagon. (b) inside the hexagon.

is solved as:

$$\begin{cases} \boldsymbol{i}_{ref} = \boldsymbol{i}_{com} & if\ (|i_{com}| \le |I|_{max}) \\ \boldsymbol{i}_{ref} = \dfrac{|I|_{max}}{|i_{com}|}\boldsymbol{i}_{com} & if\ (|i_{com}| > |I|_{max}) \end{cases} \tag{17}$$

Then the desired current increment vector from the actual current point to the reference can be expressed as:

$$\boldsymbol{i_0 i_{ref}} = \boldsymbol{i}_{ref} - \boldsymbol{i}_0 \tag{18}$$

2) FIND THE SECTOR j WHERE $i_0\, i_{ref}$ IS LOCATED

The basic of the following comparison and output voltage selection is to find out which two basic current vectors $\boldsymbol{i_0 i_{ref}}$ is between, as shown in Fig. 3. Vector products are used in this work. The vector product of $\boldsymbol{i_0 i_{ref}}$ and the basic current vector $\boldsymbol{i_0 i_j}$ can be expressed as:

$$\boldsymbol{i_0 i_{ref}} \times \boldsymbol{i_0 i_j} = (i_{dref} - i_{d0})(i_{qj} - i_{q0}) - (i_{qref} - i_{q0})(i_{dj} - i_{d0}) \tag{19}$$

The value of (19) is the length of the product and the symbol of (19) represents the direction of the product. On a two-dimensional plane, if the vector product is positive, it indicates that the second vector is clockwise in the first one and the angle is less than 180 degrees. Therefore, if the vector $\boldsymbol{i_0 i_{ref}}$ is in the sector j between the two basic current vector $\boldsymbol{i_0 i_j}$ and $\boldsymbol{i_0 i_{j+1}}$, then the following equation is satisfied:

$$(\boldsymbol{i_0 i_{ref}} \times \boldsymbol{i_0 i_j}) \cdot (\boldsymbol{i_0 i_{ref}} \times \boldsymbol{i_0 i_{j+1}}) < 0 \tag{20}$$

3) DETERMINE WHETHER i_{ref} IS INSIDE THE HEXAGON

The third step is to find out whether the reference $\boldsymbol{i}_{ref}$ can be reached within the next control period. If $\boldsymbol{i}_{ref}$ is inside the hexagon, the DPCC can be directly used to calculate the voltage reference. Otherwise, the algorithm needs to be modified. After the section j is determined in last step, the basic current vectors are decided. The geometrical description is shown in Fig. 5. Where $\boldsymbol{y}$ is the vertical foot from $\boldsymbol{i}_0$ to line: $i_j i_{j+1}$, $\boldsymbol{x}$ is the intersection of line: $i_0 i_{ref}$ and line: $i_j i_{j+1}$. The distance D from $\boldsymbol{i}_0$ to the side of the sector j is:

$$D = |i_0 y| = |(i_{d0} - i_{dj})(i_{qj+1} - i_{qj}) - (i_{q0} - i_{qj})(i_{dj+1} - i_{dj})| \tag{21}$$

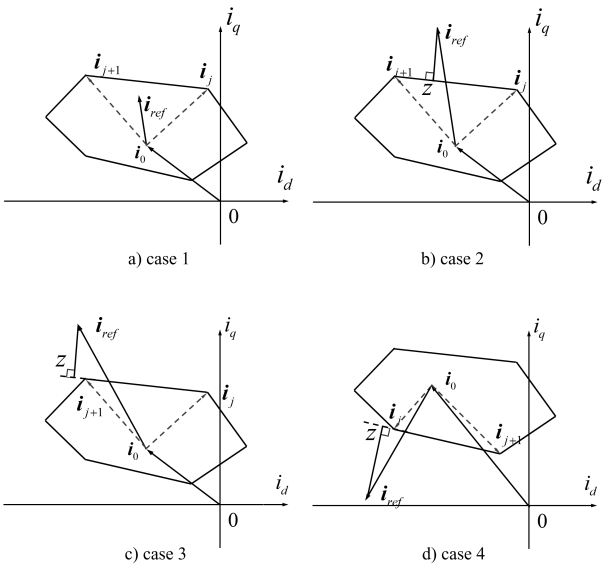

FIGURE 6. Four cases for the proposed method. (a) i_{ref} is inside the hexagon. (b) the foot point z is on the side. (c) z is on the extension of $i_j i_{j+1}$ and i_{j+1} is on the left of i_j. (d) z is on the extension of $i_j i_{j+1}$ and i_{j+1} is on the right of i_j.

The angle θ_x between the $\boldsymbol{i_0 i_{ref}}$ and $\boldsymbol{i_j i_{j+1}}$ can be obtained by:

$$\cos\theta_x = \frac{\boldsymbol{i_0 i_{ref}} \cdot \boldsymbol{i_j i_{j+1}}}{|i_0 i_{ref}||i_j i_{j+1}|} \tag{22}$$

Then the length of $|i_0 x|$ can be expressed as:

$$|i_0 x| = \frac{D}{\sin\theta_x} \tag{23}$$

If the value of $|i_0 x|$ is larger than $|i_0 i_{ref}|$, the current reference point is in the hexagon. Otherwise, the algorithm needs to be modified.

4) THE OUTPUT OF THE PROPOSED METHOD

The output signals of the conventional current controllers are the reference voltages, e.g. DPCC. As for the direct drive method, e.g. FCS-MPC, the signal is the selected voltage vector. The purpose of the proposed method is to change the current trajectory and find the nearest available current point to the reference. Therefore, the dynamic is improved even with the voltage limit because there is no saturation in the algorithm. Both MPC and DPCC are used in the algorithm which can switch fluently between each other. The output of the proposed method is divided into four cases as shown in Fig. 6.

Case 1: if $\boldsymbol{i_{ref}}$ is inside the hexagon, the point can be directly reached with DPCC. The output dq-axis reference voltages is calculated and SVPWM is used to sovle the time duration of the basic voltage vectors. Note that the SVPWM here is not limited by the inscribed circle.

Case 2: if the current reference is large, i.e. $\boldsymbol{i_{ref}}$ is outside the hexagon, the position of the vertical foot from $\boldsymbol{i_{ref}}$ to the line: $i_j i_{j+1}$ is solved. In Fig. 6, $z(i_{dz}, i_{qz})$ is the vertical foot and the following equation is satisfied:

$$\begin{cases} \dfrac{i_{qref} - i_{qz}}{i_{dref} - i_{dz}} = \dfrac{i_{dj} - i_{dj+1}}{i_{qj} - i_{qj+1}} \\ \dfrac{i_{qj} - i_{qz}}{i_{dj} - i_{dz}} = \dfrac{i_{qj} - i_{qj+1}}{i_{dj} - i_{dj+1}} \end{cases} \tag{24}$$

Solving (24), the coordinate of point $\boldsymbol{z}$ is obtained:

$$\begin{cases} i_{dz} = \dfrac{1}{h}\Big(\left(i_{qj+1} - i_{qj}\right)\left(i_{dj+1} i_{qj} - i_{dj} i_{qj+1}\right) \\ \qquad + \left(i_{dj} - i_{dj+1}\right)\left(\left(i_{dj} - i_{dj+1}\right) i_{dref} \right. \\ \qquad \left. + \left(i_{qj+1} - i_{qj}\right) i_{qref}\right)\Big) \\ i_{qz} = \dfrac{1}{h}\Big(-\left(i_{qj} - i_{qj+1}\right)^2 i_{qref} + \left(i_{dj} - i_{dj+1}\right) \\ \qquad \left(- i_{dj+1} i_{qj} + i_{dref}\left(i_{qj} - i_{qj+1}\right) + i_{dj} i_{qj+1}\right)\Big) \end{cases} \tag{25}$$

where

$$h = (i_{dj} - i_{dj+1})^2 - (i_{qj} - i_{qj+1})^2$$

If the foot $\boldsymbol{z}$ is on the line segment between $\boldsymbol{i_j}$ and $\boldsymbol{i_{j+1}}$, it is the nearest reachable current point. Then the new current command point is upated with: $\boldsymbol{i_{ref}} = \boldsymbol{z}(i_{dz}, i_{qz})$.

Case 3: if $\boldsymbol{i_{ref}}$ and $\boldsymbol{i_z}$ are both outside the hexagon, the nearest point will be the vertex of the current hexagon. Fig. 6 (c) represents the condition that $\boldsymbol{i_{j+1}}$ is on the left of the $\boldsymbol{i_j}$. If $\boldsymbol{i_z}$ is on the left of $\boldsymbol{i_{j+1}}$, the selected current vector is $\boldsymbol{i_0 i_{j+1}}$. The relative output basic voltage vector is $j + 1$th. Otherwise, the vector will is jth as (26). The voltage vector can be operated directly on the motor, like MPC, to obtain the fast dynamic.

$$\begin{cases} j_{out} = j + 1 & (if\ i_{dz} < i_{dj+1}) \\ j_{out} = j & (if\ i_{dz} > i_{dj}) \end{cases} \tag{26}$$

Case 4: if $\boldsymbol{i_{j+1}}$ is on the right of the $\boldsymbol{i_j}$ as shown in Fig. 6 (d), the conclusion is opposite as (27).

$$\begin{cases} j_{out} = j + 1 & (if\ i_{dz} > i_{dj+1}) \\ j_{out} = j & (if\ i_{dz} < i_{dj}) \end{cases} \tag{27}$$

In this way, four cases switch based on the position of $\boldsymbol{i_{ref}}$ and $\boldsymbol{i_z}$. The current point moves towards the reference with the fastest speed in every period.

V. VALIDATION

Several experiments are performed on a SPMSM platform, as shown in Fig. 7 to validate the effectiveness of the proposed method. The rated values and parameters of the PMSM are given in Table 1. The test SPMSM is in the power-driven state and driven by a servo motor which is in the power generation state. The servo motor is controlled in speed mode by a commercial controller and the SPMSM is controlled in current mode to operate the proposed method. The DC-link voltage of the inverter for SPMSM is supplied by a programmable DC power, thus, the voltage can be tuned for different experiments. The current control methods are carried out on a 32-bit floating-point DSP TMS320F28335. The sampling

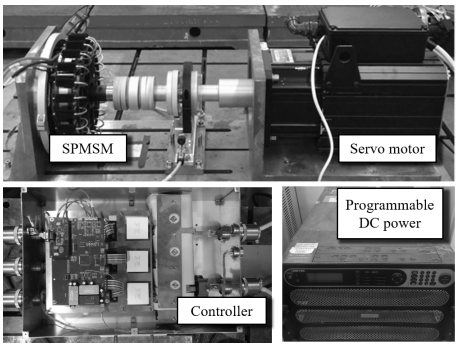

FIGURE 7. Experiment setup.

TABLE 1. Nominal PMSM parameters.

Symbol	Quantity	Quantity
n_{rated}	Rated speed	$1700rpm$
$T_{e,rated}$	Rated torque	$24Nm$
I_{rated}	Rated current	$29.1A$
R_s	Stator resistance	0.04Ω
L	Stator inductance	$0.72mH$
ψ_f	Permanent-magnet flux linkage	$0.05Wb$
n_p	Pole pairs	11
$f_{e,rated}$	Rated electrical angular speed	$311.7Hz$

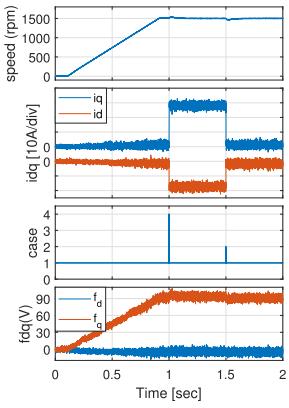

FIGURE 8. Experiment results at 1500rpm, $i_d = -15A$, $i_q = 29A$.

frequency of the current loop is set as 10 kHz, which is equaled to the switching frequency of insulated-gate-bipolar-transistors (IGBTs). The dead time of the power devices is set as $1\mu s$. The rotor position and the currents of phase A/B are measured by a resolver and current sensors. An external 12-bit D/A converter is applied in the hardware circuits. The digital variables are converted to analogy signals and shown on a scope DLM2034 in the experiments of this work. In the following experiments, the dq-axis current reference are used directly instead of a torque command.

A. PERFORMANCE AT STEADY STATES

First, the experiment results of the proposed method at steady states with accurate parameters are presented in Fig. 8, of which the zoomed waveforms are shown in Fig. 9. The servo motor accelerates from 0 to 1500rpm and the current command point are set as $(-15A, 29A)$ at 1s and $(0A, 0A)$ at 1.5s. The condition that the reference point is beyond the max

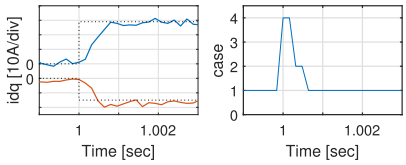

FIGURE 9. Zoomed waveforms of Fig. 8.

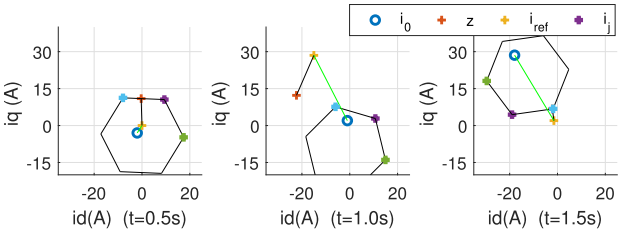

FIGURE 10. Experiment results on the current plane.

current circle I_{max} is not concern in this work, because it can not be reached without violating the limit. The currents track the reference fast and a small error, about $-2A$, exists in i_d due to the delays of the system. The estimated disturbances are shown at the bottom of Fig. 8. f_q increases with the speed when the motor accelerates. The value is equal to the back-EMF while f_d is zero when there is no parameter mismatches. In the begining of the experiment, the current command point is the origin which is within the current hexagon as shown in Fig. 10 (a). The proposed method operates at case 1. The hexagons are calculated based on the sampled currents, rotor speed and position at the certain instant. When a large reference is commanded, the points $\boldsymbol{i}_{ref}$ and $\boldsymbol{z}$ are located outside the hexagon. Due to the position of the points, case 4 is first operated (as shown in Fig. 10 (b)) and then turns to case 2. Note that cases 2, 3 and 4 are all possible when $\boldsymbol{i}_{ref}$ is outside the hexagon. It depends on the angle of the hexagon, which is related to the position of rotor. When the current is close to the command point, the case return to case 1. When the current reference returns to the origin, the method is first operated in case 2 as Fig. 10 (c). It can be seen that the algorithm can switch fluently to select the optimal case for the fast dynamic.

B. PERFORMANCE COMPARISON WITH DIFFERENT METHODS

In this section, the experiments of three methods: DPCC, FCS-MPC, the proposed predictive method are performed and compared. The motor is rotated at rated speed ($1700rpm$) and then step reference i_q is operated. First, the DC-voltage is set as 200V and the results are shown in Fig. 11. It can be seen that, the dynamics of FCS-MPC and the proposed predictive method are faster than DPCC. However, the current ripple of FCS-MPC is much larger than the proposed method. Moreover, it is the drawback of MPC that the d-axis current can not be controlled precisely. Since only the eight basic voltage vectors are used, the currents are always in the process of large scale adjustment. In Fig. 11 (b), the current trajectory from the origin to the reference of three methods are shown.

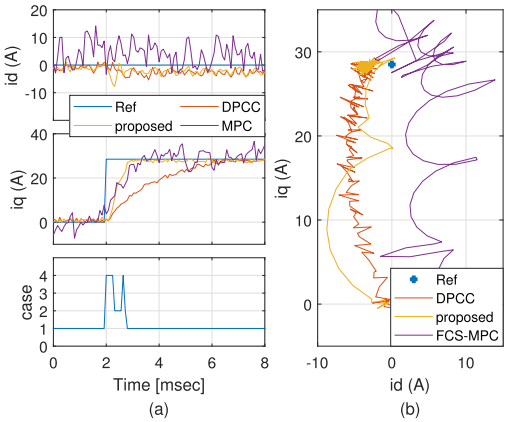

FIGURE 11. Experiment results with 200V DC-voltage. (a) current waveforms. (b) current trajectories.

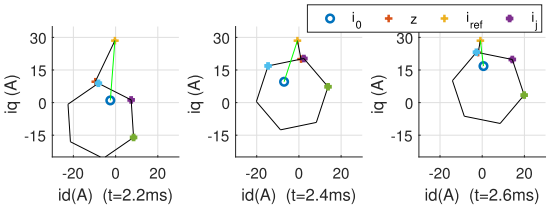

FIGURE 12. The current plane at different instants with 200V DC-voltage.

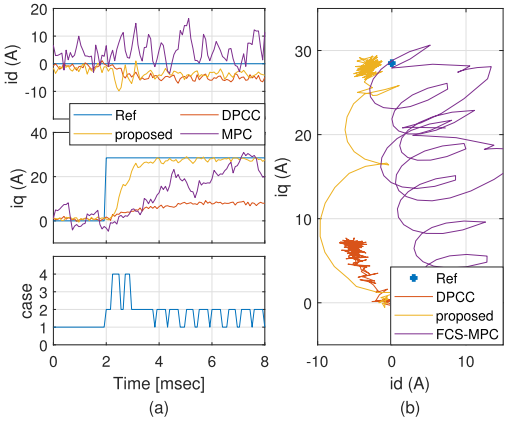

FIGURE 13. Experiment results with 185V DC-voltage. (a) current waveforms. (b) current trajectories.

Since it takes longer time to reach the current command, the curve of DPCC contains more points. A large negtive i_d occurs in the proposed method due to the optimal trajectory as shown in Fig. 12. $\boldsymbol{z}$ is on the left of the origin in the first periods and the currents are controlled to track $\boldsymbol{z}$ or the blue point $\boldsymbol{i_{jc1}}$ by case 2 or 4. If the point z locates on the side of the hexagon, the method switches to case 2.

The results with lower DC-link voltage $185V$ are shown in Fig. 13. In this condition, the currents of DPCC can not track the references due to the serious saturation and the limit of voltage modulation. It aslo takes longer time for FCS-MPC to track the reference. However, the currents of the proposed method can still show good performance.

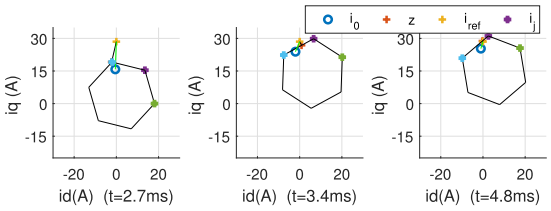

FIGURE 14. The current plane at different instants with 185V DC-voltage.

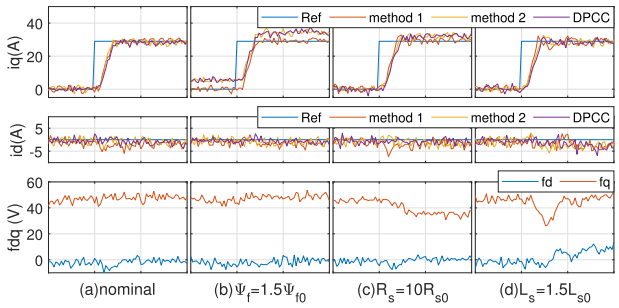

FIGURE 15. Experiment results with different parameters.

The negative i_d reduces the $d-$axis voltage and the combination of FCS-MPC increases the utilize of the DC-link voltage. Because the current hexgons with lower voltage (as shown in Fig. 14) are smaller than those of the Fig. 12, the $\boldsymbol{i}_0$ and $\boldsymbol{i}_{ref}$ locate close to the side of the hexagon when the current point is near the reference with large back-EMF. The current reference point $\boldsymbol{i}_{ref}$ goes beyond the hexagon more easily with the current harmonic and the rotor rotation, so that the case switches between 1 and 2 frequently.

C. PERFORMANCE WITH PARAMETER MISMATCH

In this section, several experiments with different parameters are performed. Since the real parameter of SPMSM is hard to change in a short period, instead, the parameters used in algorithm are changed for comparison. The performance of the proposed method with the MHE (here named method 1) is compared with that of DPCC and the proposed current control without MHE (here named method 2). The results are shown in Fig. 15. The motor speed is 800rpm and the performance of three methods shows similar performance with the nonimal parameters in (a). When the flux is set as $1.5\psi_{f0}$, i_q of DPCC and method 2 deviate from the reference value in both no load and load condition. However, the currents of method 1 do not change because the flux is not used in the algorithm and the voltage terms are replaced by f_d, f_q. When the resistance changes to $10R_{s0}$ in (c), i_q of DPCC and method 2 become larger than the reference after the command is operated. While the current performance of the method 1 is hardly influenced because the voltage error caused by the resistance variation is compensated by the estimated disturbance. While the variation of inductance influence the $d-$axis current most, with large i_q according to (8). It can be seen that, the accuracy of flux linkage affects the current tracking performace more seriously, since the back-EMF is usually larger than the

voltage drop on the impedance when the motor is rotating. With the help of MHE, the flux is eliminated in the algorithm and the robustness of the proposed method against the parameter mismatches increases. Note that the MHE is more sensitive to the inductance variation and an overshoot occurs in method 1 when the current change in (d).

VI. CONCLUSION

This paper proposes a predictive current trajectory control method with moving horizon estimator. The proposed current control strategy combines FCS-MPC and DPCC, and finds the optimal available current point with geometrical method on the current plane. The saturation of the current loop is reduced with the command point calculation and the dynamic at the voltage limit is much improved with the help of the combination. The output of the algorithm is divided into four cases, and the control strategy can switch smoothly among them. MHE can estimate the disturbance, including the back-EMF, accurately. With the estimated disturbance, the flux is eliminated in the algorithm and the robustness to parameter variations increases. The effectiveness of the proposed method is validated through several comparible experiments.

REFERENCES

[1] Y.-C. Kwon, S. Kim, and S.-K. Sul, "Voltage feedback current control scheme for improved transient performance of permanent magnet synchronous machine drives," *IEEE Trans. Ind. Electron.*, vol. 59, no. 9, pp. 3373–3382, Sep. 2012.
[2] F. Wang, X. Mei, J. Rodriguez, and R. Kennel, "Model predictive control for electrical drive systems-an overview," *CES Trans. Elect. Mach. Syst.*, vol. 1, no. 3, pp. 219–230, Sep. 2017.
[3] Y. Wang, S. Tobayashi, and R. D. Lorenz, "A low switching frequency flux observer and torque model of deadbeat direct torque and flux control on induction machine drives," *IEEE Trans. Ind. Appl.*, vol. 51, no. 3, pp. 2255–2267, May 2015.
[4] M. H. Vafaie, B. M. Dehkordi, P. Moallem, and A. Kiyoumarsi, "Improving the steady–state and transient–state performances of PMSM through an advanced deadbeat direct torque and flux control system," *IEEE Trans. Power Electron.*, vol. 32, no. 4, pp. 2964–2975, Apr. 2017.
[5] R. S. Dastjerdi, M. A. Abbasian, H. Saghafi, and M. H. Vafaie, "Performance improvement of permanent–magnet synchronous motor using a new deadbeat–direct current controller," *IEEE Trans. Power Electron.*, vol. 34, no. 4, pp. 3530–3543, Apr. 2019.
[6] J. S. Lee and R. D. Lorenz, "Deadbeat direct torque and flux control of IPMSM drives using a minimum time ramp trajectory method at voltage and current limits," *IEEE Trans. Ind. Appl.*, vol. 50, no. 6, pp. 3795–3804, Nov. 2014.
[7] Z. Zhou, C. Xia, Y. Yan, Z. Wang, and T. Shi, "Torque ripple minimization of predictive torque control for PMSM with extended control set," *IEEE Trans. Ind. Electron.*, vol. 64, no. 9, pp. 6930–6939, Sep. 2017.
[8] W. Xie, X. Wang, F. Wang, W. Xu, R. M. Kennel, D. Gerling, and R. D. Lorenz, "Finite-control-set model predictive torque control with a deadbeat solution for PMSM drives," *IEEE Trans. Ind. Electron.*, vol. 62, no. 9, pp. 5402–5410, Sep. 2015.
[9] Y. Xu, Q. Zhou, and B. Zhang, "A model predictive torque control strategy of pmsm with torque deadbeat duty cycle control," in *Proc. IEEE 8th Int. Power Electron. Motion Control Conf. (IPEMC-ECCE Asia)*, May 2016, pp. 782–785.
[10] S.-M. Sue and C.-T. Pan, "Voltage-constraint-tracking-based field–weakening control of IPM synchronous motor drives," *IEEE Trans. Ind. Electron.*, vol. 55, no. 1, pp. 340–347, Jan. 2008.
[11] T.-S. Kwon and S.-K. Sul, "Novel anti-windup of a current regulator of a surface-mounted permanent-magnet motor for flux-weakening control," in *Proc. 14th IAS Annu. Meeting Conf. Rec. Ind. Appl. Conf.*, vol. 3, Oct. 2005, pp. 1813–1819.
[12] P.-Y. Lin and Y.-S. Lai, "Voltage control technique for the extension of DC–link voltage utilization of finite–speed SPMSM drives," *IEEE Trans. Ind. Electron.*, vol. 59, no. 9, pp. 3392–3402, Sep. 2012.
[13] H. M. Flieh, R. D. Lorenz, E. Totoki, S. Yamaguchi, and Y. Nakamura, "Dynamic loss minimizing control of a permanent magnet servomotor operating even at the voltage limit when using deadbeat–direct torque and flux control," *IEEE Trans. Ind. Appl.*, vol. 55, no. 3, pp. 2710–2720, May 2019.
[14] J. S. Lee, R. D. Lorenz, and M. A. Valenzuela, "Time–optimal and loss–minimizing deadbeat–direct torque and flux control for interior permanent–magnet synchronous machines," *IEEE Trans. Ind. Appl.*, vol. 50, no. 3, pp. 1880–1890, May 2014.
[15] H. Ghasemi and S. Vaez-Zadeh, "A very fast direct torque control for permanent magnet synchronous motors start up," in *Proc. Can. Conf. Elect. Comput. Eng.*, Nov. 2004, pp. 1673–1677.
[16] J. Lemmens, P. Vanassche, and J. Driesen, "PMSM drive current and voltage limiting as a constraint optimal control problem," *IEEE J. Emerg. Sel. Topics Power Electron.*, vol. 3, no. 2, pp. 326–338, Jun. 2015.
[17] L. Yang, R. Gao, W. Yu, and I. Husain, "A geometrical linearization approach for salient-pole PMSM optimal voltage/current constrained control over whole speed range," in *Proc. IEEE Energy Convers. Congr. Exposit. (ECCE)*, Oct. 2017, pp. 350–356.
[18] J. Richter and M. Doppelbauer, "Predictive trajectory control of permanent–magnet synchronous machines with nonlinear magnetics," *IEEE Trans. Ind. Electron.*, vol. 63, no. 6, pp. 3915–3924, Jun. 2016.
[19] V. Smidl, S. Janous, Z. Peroutka, and L. Adam, "Time-optimal current trajectory for predictive speed control of PMSM drive," in *Proc. IEEE Int. Symp. Predictive Control Electr. Drives Power Electron. (PRECEDE)*, Sep. 2017, pp. 83–88.
[20] H. Qin, M. Dou, Y. Wang, and L. Yan, "Fast response deadbeat current control for PMSM," in *Proc. IEEE Int. Symp. Predictive Control Electr. Drives Power Electron. (PRECEDE)*, May 2019, pp. 1–5.
[21] Y.-R. Mohamed, "Design and implementation of a robust current–control scheme for a PMSM vector drive with a simple adaptive disturbance observer," *IEEE Trans. Ind. Electron.*, vol. 54, no. 4, pp. 1981–1988, Aug. 2007.
[22] M. Abdelrahem, C. M. Hackl, Z. Zhang, and R. Kennel, "Robust predictive control for direct–driven surface–mounted permanent–magnet synchronous generators without mechanical sensors," *IEEE Trans. Energy Convers.*, vol. 33, no. 1, pp. 179–189, Mar. 2018.
[23] H. Yang, Y. Zhang, J. Liang, B. Xia, P. D. Walker, and N. Zhang, "Deadbeat control based on a multipurpose disturbance observer for permanent magnet synchronous motors," *IET Electric Power Appl.*, vol. 12, no. 5, pp. 708–716, May 2018.
[24] M. Yang, X. Lang, J. Long, and D. Xu, "Flux immunity robust predictive current control with incremental model and extended state observer for PMSM drive," *IEEE Trans. Power Electron.*, vol. 32, no. 12, pp. 9267–9279, Dec. 2017.
[25] F. Valencia, J. D. Lopez, A. Marquez, and J. J. Espinosa, "Moving horizon estimator for measurement delay compensation in model predictive control schemes," in *Proc. IEEE Conf. Decision Control Eur. Control Conf.*, Dec. 2011, pp. 6678–6683.
[26] L. Ji, J. B. Rawlings, W. Hu, A. Wynn, and M. Diehl, "Robust stability of moving horizon estimation under bounded disturbances," *IEEE Trans. Autom. Control*, vol. 61, no. 11, pp. 3509–3514, Nov. 2016.
[27] L. Zhou and Y. Wang, "Speed sensorless state estimation for induction motors: A moving horizon approach," in *Proc. Amer. Control Conf. (ACC)*, Jul. 2016, pp. 2229–2234.
[28] F. Toso, D. Da Ru, P. Alotto, and S. Bolognani, "A moving horizon estimator for the speed and rotor position of a sensorless PMSM drive," *IEEE Trans. Power Electron.*, vol. 34, no. 1, pp. 580–587, Jan. 2019.
[29] F. Toso, M. De Soricellis, M. Preindl, and S. Bolognani, "Moving horizon estimator of PMSM N Onlinearities," in *Proc. 44th Annu. Conf. IEEE Ind. Electron. Soc.*, Oct. 2018, pp. 583–588.
[30] K. Li and Y. Wang, "Maximum torque per ampere (MTPA) control for IPMSM drives based on a variable-equivalent-parameter MTPA control law," *IEEE Trans. Power Electron.*, vol. 34, no. 7, pp. 7092–7102, Jul. 2019.

GENJI PEI received the B.E. degree from the Harbin Institute of Technology (HIT), Harbin, China, in 2016, where he is currently pursuing the Ph.D. degree with the School of Electrical Engineering and Automation. He worked as a Joint Ph.D. Student with the Institute for Electrical Drive Systems and Power Electronics, Technical University of Munich, German, from 2018 to 2019. His research interests include parameter identification, robust control, and model predictive control of PMSM.

LIYI LI (Senior Member, IEEE) received the B.E., M.E., and D.E. degrees from the Harbin Institute of Technology (HIT), Harbin, China, in 1991, 1995, and 2001, respectively.

Since 2004, he has been a Professor with the School of Electrical Engineering and Automation, HIT. In 2013, he became the Yangtze Fund Scholar Distinguished Professor. He has been supported by the National Science Fund for Distinguished Young Scholars. He has authored or coauthored more than 110 technical articles. He holds 50 patents. His research interests include design, drive and control of linear motors, design, and drive of high-speed/power density permanent magnet machines.

XIAONAN GAO was born in Liaoning, China, in 1990. He received the B.S. and M.S. degrees in electrical engineering from the Dalian University of Technology (DUT), Dalian, China, in 2013 and 2016, respectively. He is currently pursuing the Ph.D. degree with the Institute for Electrical Drive Systems and Power Electronics, Technical University of Munich, Germany.

His research interests include power electronics and electrical drives, predictive control, and multilevel converters.

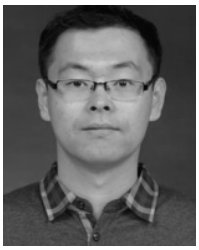

JIAXI LIU received the B.E., M.E., and Ph.D. degrees from the Harbin Institute of Technology (HIT), Harbin, China, in 2004, 2006, and 2010, respectively.

Since 2015, he has been an Associate Professor with the School of Electrical Engineering and Automation, HIT. His research interests include high-speed motor drive, and servo control in the nano-field. He holds six patents.

RALPH KENNEL (Senior Member, IEEE) was born in Kaiserslautern, Germany, in 1955. He received the Diploma and Dr.Ing. (Ph.D.) degrees from the University of Kaiserslautern, in 1979 and 1984, respectively.

Since 2008, he has been a Professor of electrical drive systems and power electronics with Technische Universität Muenchen, Germany. His main interests include sensorless control of ac drives, predictive control of power electronics, and hardware-in-the-loop systems.

Dr. Kennel is currently a Fellow of IEE and a Chartered Engineer in the U.K. Within IEEE, he is a Treasurer of the Germany Section and the ECCE Global Partnership Chair of the Power Electronics Society (PELS).